Dual-Band Omnidirectional and Circularly Polarized Slotted Waveguide Array Antenna for Satellite Telemetry and Telecommand

Ceyhan Turkmen, *Student Member, IEEE*, and Mustafa Secmen, *Senior Member, IEEE*

***Abstract*—In this letter, the design and 3-D-printed manufacturing of an omnidirectional and circularly polarized dual-band antenna for telemetry/telecommand (TMTC) applications in satellite communication on space segment are described. The antenna consists of slotted arrays on the circular waveguide with radially outward metallic disks and choke structures on these disks to improve the omnidirectionality and circular polarization performances. As the main novelty of the antenna design, the structure is fed with only one rectangular waveguide; therefore, the proposed antenna can be considered as a transceiver antenna. The design and simulations of the antenna and measurement results for 3-D-printed manufacturing are given at Ku-band. A 10 dB return loss bandwidth is found to be 500 MHz both for telemetry and telecommand bands having center frequencies of 12 and 14 GHz, respectively. Besides, the maximum axial ratio and minimum gain within 65° beamwidth are obtained as 3 dB and −5 dBi, respectively, which are sufficient for the omnidirectional and circularly polarized antenna providing TMTC communication in satellite systems.**

***Index Terms*—3-D-printed antennas, circular polarization, omnidirectional antennas, satellite telemetry/telecommand (TMTC), slotted waveguide array.**

I. Introduction

DURING the time between launch and placement of satellites in the proper orbit, its position and aspect angle relative to the ground station can be random due to the possible vibrations and other force effects in the passage through atmosphere. However, the communication between the ground station and the satellite must be uninterrupted for satellite's position and other telemetry (TM) information. For this reason, TM (transmitter) and telecommand (TC) (receiver) antennas on the satellite platform should be able to transmit and receive electromagnetic waves from all directions to ensure a two-way communication. This communication is called as telemetry and telecommand (TMTC) [1], [2]. The other problem on signal level of the communication is polarization mismatch, which is caused by variation in the aspect angle. Therefore, TMTC antennas on the satellite segment are selected as circularly polarized to minimize these losses as possible.

Manuscript received August 1, 2021; accepted August 19, 2021. Date of publication September 1, 2021; date of current version November 16, 2021. This work was supported in part by the Scientific and Technological Research Council of Turkey (TUBITAK) under Grant 119E265. *(Corresponding author: Mustafa Secmen.)*

The authors are with the Department of Electrical and Electronics Engineering, Yasar University, 35100 Bornova, Turkey (e-mail: ceyhan.turkmen@yasar.edu.tr; mustafa.secmen@yasar.edu.tr).

Digital Object Identifier 10.1109/LAWP.2021.3109030

The isotropic radiation characteristics being achieved with one antenna is a hypothetical concept. Isotropic radiation pattern is generally satisfied by using two wide coverage antennas and one omnidirectional antenna [3]–[9] or two hemispherical antennas [10]–[13]. The combination of these antennas gives not perfect isotropic characteristics but an approximate nondirection pattern if each antenna provides about 65°–70° beamwidth [14]. In the literature, there are many omnidirectional circularly polarized antennas, which uses dielectric materials [15]–[23]. However, for geostationary (GEO) satellites, the satellite can be 36 000 km away from Earth such that the transmitted RF power can be as high as on the order of 100 W [24]. Therefore, antenna designs with microstrip lines [15]–[19], coaxial lines/pins [3], [7], [20], and dielectric materials [21]–[23] are not proper for high power applications due to thermal and mechanical problems. The waveguide fed omnidirectional and circularly polarized antennas used to solve the mentioned problems are generally single-band antennas [5], [9]. Therefore, two separate antennas (one antenna for TM frequencies and one identical antenna for TC frequencies) should be used. The antenna designs in [4] can be still considered as two "single-band" antennas such TM and TC channels have different feeds (waveguides with complex turnstile-junction structure or coaxial lines). Besides, the circularly polarized version in [4] is fed by coaxial lines.

In this letter, to the best of our knowledge, a dual-band omnidirectional and circularly polarized waveguide antenna is presented for the first time. The antenna contains one common rectangular waveguide feed and no dielectric material. Therefore, number of TMTC antennas in space segment becomes one, which provides low volume and low mass. The antenna whose design is given in Section II is verified for Ku-band with a 3-D printing. The simulation and measurement results show that minimum 10 dB return loss and −5 dBi gain, and at most 3 dB AR are obtained over 500 MHz bandwidth around TM and TC center frequencies of 12 and 14 GHz.

II. Antenna Design

The waveguide antenna structure shown in Fig. 1 consists of two parts: feed part and radiation part. In the radiation part, two sections of 45° slotted arrays exist on circular waveguides with different radii. Upper circular waveguide with smaller radii and upper slots are for higher (TC) frequencies, and lower slots with relatively larger circular waveguide gives radiation at lower (TM) frequencies. The slots are placed in a cylindrically symmetric way in geometry for omnidirectional pattern. However, in addition to geometric symmetry, the slots should be excited with a circularly symmetric field/mode, which is TM_{01} mode

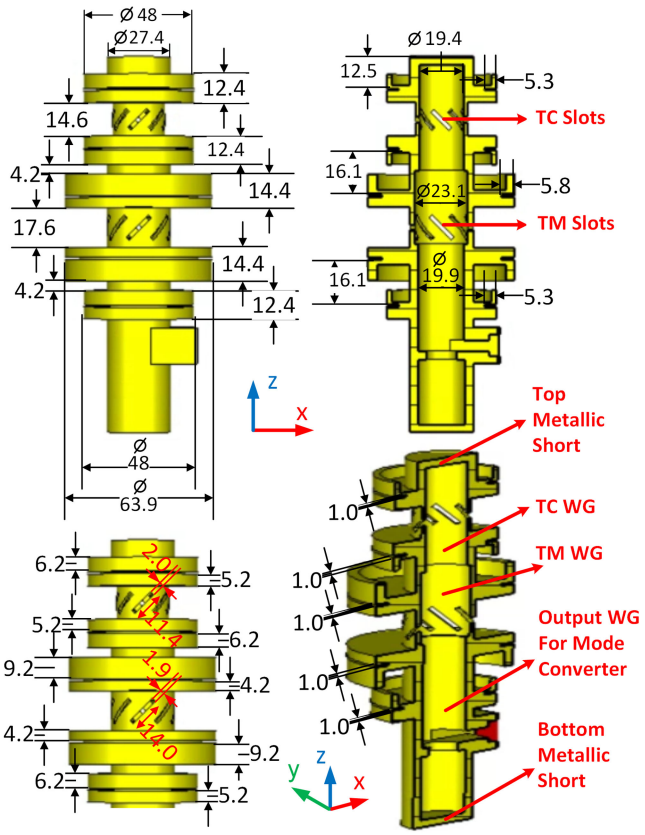

Fig. 1. Structure of the designed antenna and its dimensions in millimeter.

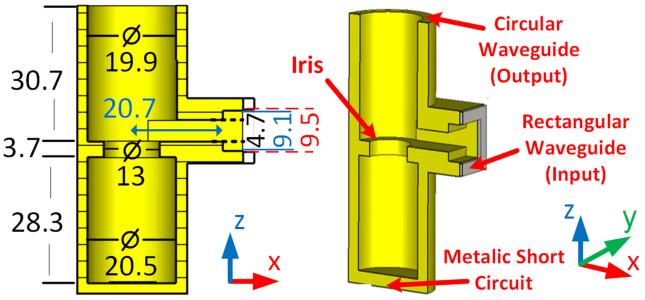

Fig. 2. Designed dual-band rectangular TE_{10} mode to circular TM_{01} mode converter and its dimensions in millimeter.

in circular waveguide. Therefore, the feed part below slotted sections are used as a dual-band mode converter, which makes the mode conversion from the input rectangular waveguide TE_{10} mode to the circular waveguide TM_{01} mode at the output circular waveguide with diameter of 19.9 mm in Fig. 1. The disks extending radially away from circular waveguides and chokes on the disks are used to improve the AR performance of the antenna in both frequency bands.

A. Dual-Band TE_{10} Mode—Circular TM_{01} Mode Converter

The proposed structure shown in Fig. 2, which operates dual band at 12 GHz (TM) and 14 GHz (TC) center frequencies, is designed to provide transition from the rectangular waveguide TE_{10} mode to the circular waveguide TM_{01} mode. The rectangular waveguide (port 1) is a standard WR-75 waveguide

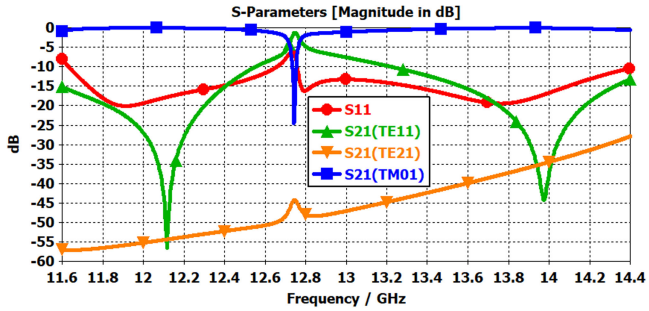

Fig. 3. Simulated S-parameters of the dual-band rectangular TE_{10} mode to circular TM_{01} mode converter.

(a = 19.05, b = 9.525 mm) in Ku-band. The diameter of the output circular waveguide (port 2) is 19.9 mm, which allows the transmission of TM_{01} mode and attenuates the circular TE_{21} and other higher order modes by keeping cutoff frequencies of these modes above 14.3 GHz. For the suppression of the dominant TE_{11} mode in the circular waveguide, the distance between the bottom short circuit and rectangular waveguide should be $0.75\lambda_{g,TE11}$ as described in [9] for a single-band design. Besides, the diameter of lower circular waveguide should be $0.5\lambda_{g,TM01}$ for transmission of TM_{01} mode. Although dimensions of 28.3 and 20.5 mm given in Fig. 2 almost satisfy these electrical lengths at TM frequencies, an iris with a thickness of 3.7 mm and a diameter of 13 mm is added to enhance the suppression of TE_{11} mode at TC frequency band. Two steps in *E*-plane on rectangular waveguide are also added to improve S_{11} values.

All dimensions in Fig. 2 are optimized with CST MWS and the corresponding simulation S-parameters are given in Fig. 3. From the results, at least 12 dB return loss, at least 16 dB and 30 dB suppression values for TE_{11} and TE_{21} modes, and at most 0.4 dB insertion loss for the TM_{01} mode are obtained within about 700 MHz bandwidth for both bands (11.7–12.4 GHz for TM band, and 13.6–14.3 GHz for TC band).

B. Sections of Slotted Arrays and Disks/Chokes

As in Fig. 1, there are three circular waveguide sections above the rectangular waveguide where the lowermost waveguide is output waveguide of the mode converter in Section II. Middle and upper waveguides (TM and TC WG in Fig. 1) each having eight identical 45° inclined slots belong to TM and TC sections. From results in Fig. 3, modes except the TM_{01} mode are assumed to be sufficiently suppressed such that the design of the antenna is considered only with the TM_{01} mode in circular waveguides.

For the TM_{01} mode, radiation impedances of the slots are modeled as series in the equivalent circuit; therefore, the distance between top metallic short and the center of TC slots is arranged as $0.5\lambda_{g,TM01}$ at 14 GHz (almost 24 mm) to give maximum radiation [14]. TM frequencies cannot propagate within the upper circular waveguide with the diameter of 19.4 mm since the cutoff frequency of the TM_{01} mode is higher than TM frequencies for this waveguide, which prevents the leakage of TM frequencies from TC slots. Therefore, the boundary region between TM and TC circular waveguides can be modeled as short circuit for TM frequencies. Similar to TC slots, distance between the boundary region and center of TM slots is selected as $0.5\lambda_{g,TM01}$ at 12 GHz (almost 25 mm) to give maximum radiation. The length

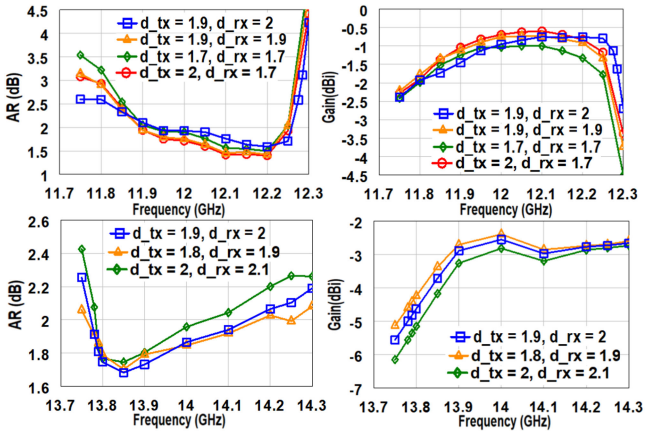

Fig. 4. Parametric analysis of the proposed antenna.

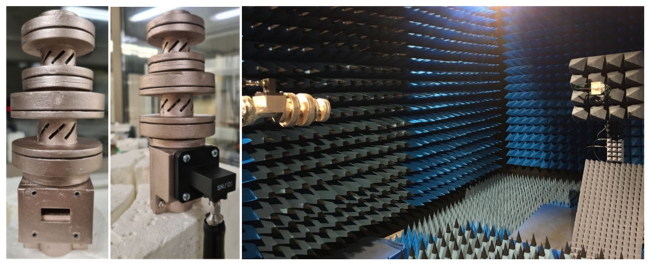

Fig. 5. Photographs of 3-D-printed prototype of the antenna in the reflection coefficient and radiation pattern measurements.

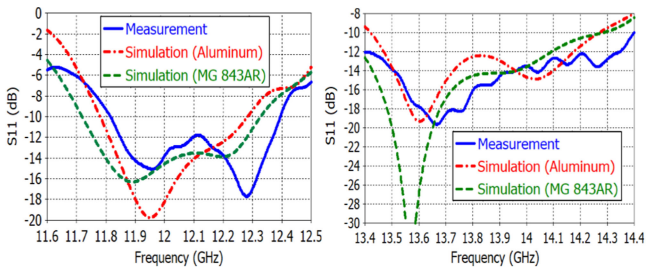

Fig. 6. S_{11} values of the proposed antenna (simulation and measurement).

and width of the slots being cut in a cylindrically symmetric way, are chosen almost $\lambda_0/2$ and $\lambda_0/20$ to be consistent with thin half wavelength dipole model at 12 and 14 GHz for TM and TC slots.

The main problem in the design is the leakage of TC frequencies from TM slots. The leakage impedance for TM slots at TC frequencies is added in series to impedance transformed from top short/TC slots to the region of TM slots. Therefore, the leakage impedance should be minimized, and the transformed impedance should be maximized to decrease the leakage of TC frequencies from TM slots as possible. The slot length of $\lambda_0/2$ at 12 GHz for TM slots in TM waveguide becomes off-resonance at 14 GHz; therefore, the leakage impedance from TM slots for TC frequencies is small. Besides, the path length between top short and the center of TM slots is arranged to give almost $1.75\lambda_{g,\mathrm{TM01}}$ at 14 GHz where 25 mm distance between the boundary region and center of TM slots is almost $0.75\lambda_{g,\mathrm{TM01}}$ at 14 GHz. Therefore, this transformation gives very high impedance at the region of TM slots minimizing the leakage radiation.

Without the radial disks in the antenna structure, the antenna has 45° slant linear polarization. As described in [5] and [9], radial disks provide 90° phase shift left-hand circular polarization (LHCP) in Fig. 1 at the aperture of the disk between horizontally and vertically polarized waves, which propagates with TE_1 and TEM modes in the disk, respectively. The radius and height of the disks are calculated from the expression (3) and explanations in [9].

To improve the AR bandwidth of the antenna, both axial and radial chokes are inserted with depth values of $\lambda_0/4$ at TM and TC sections. Choke dimensions have little effect on S_{11} and gain.

The dimensions of the antenna given in Fig. 1 are optimized with CST MWS. In the parametric analysis, the dimension (target) resolution is taken as 0.1 mm, which is also the resolution of the 3-D printer. Among all parameters, the length and width values of TM and TC slots ($l\_tx = 14.0$ mm, $l\_rx = 11.4$ mm, $d\_tx = 1.9$ mm, and $d\_rx = 2$ mm) are found to affect impedance, gain, and AR performances most with 0.1 mm resolution. Due to the limited space, only the effects of width values (*d_tx and d_rx*) of TM and TC slots on AR and gain performances are demonstrated. In Fig. 4, the highest AR and lowest gain (LG) values within 65° elevation beamwidth are given. Although other parametric values may provide better performances at the middle region of targeted bands, the optimized values give better performances especially at edge frequencies. For instance, maximum AR values at 11.75 and 11.8 GHz are lower than 3 dB only for the optimized values, which increases the bandwidth of the antenna at TX band. The length values of TM and TC slots (*l_tx*, *l_rx*) are observed to shift resonant frequencies and impedance band.

III. 3-D-Printed Prototype and Performance Results

As being a popular manufacturing technique for antennas in recent years [25], [26], 3-D-printed prototype of the designed antenna in Fig. 1 is manufactured. The antenna as final product should be manufactured with aluminum and CNC milling for the usage in high power space applications where CST simulations in Section II are performed with aluminum material. However, for the purpose of obtaining measurement results with fast and low-cost production, 3-D-printed manufacturing with polylactic acid (PLA) as dielectric material is performed. A metal spray coating with MG Chemicals 843AR aerosol [27] is applied on the 3-D-printed structure. The silver coated copper aerosol has conductivity of approximately $\sigma = 2.5 \times 10^5$ S/m resulting in skin depth value of about a few at TM and TC frequencies. Therefore, the thickness of about 100 μm expected with three coats performed in the coating process of the manufacturing is quite enough as compared to skin depth. The photographs of the 3-D-printed prototype of the antenna are depicted in Fig. 5 along with S_{11} and pattern measurements.

The simulated and measured reflection coefficient (S_{11}) results are given in Fig. 6 where measurements are performed with Anritsu MS2028C VNA and Lieder WR75 waveguide calibration kit in the Antennas and Microwave Laboratory, Yasar University. The simulation and measurements are in good agreement that the impedance bandwidth of $S_{11} < -10$ dB is measured more than 500 MHz around 12 and 14 GHz.

From Fig. 6, while about 500 MHz bandwidth (11.8–12.3 GHz) from simulation with aluminum (Al) and about 600 MHz

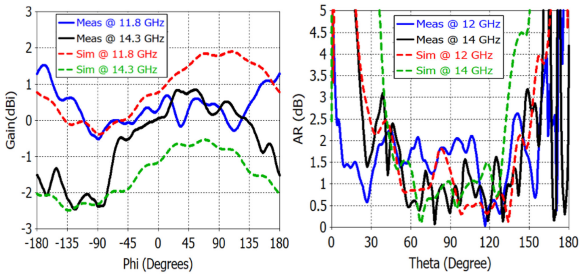

Fig. 7. Simulated (dashed) and measured (solid) azimuth gain patterns ($\theta = 90°$) of the antenna at 11.8 and 14.3 GHz (left figure). The simulated (dashed) and measured (solid) elevation axial ratio patterns ($\phi = 45°$) of the antenna at 12 and 14 GHz (right figure).

bandwidth (11.8–12.4) from measurement are obtained at the TM band, 850 MHz bandwidth (13.43–14.28 GHz) for simulations and more than 1 GHz bandwidth for measurement are found at TC band. S_{11} values from simulation with MG Chemicals 843AR are also given in Fig. 6 where these values fit to measurement results better than the ones with aluminum as expected. The slight differences (shifts) between simulation and measurement responses are due to production errors possibly coming from slots' length.

The radiation pattern measurements are realized at Spherical Near Field Measurement System of Antenna Test and Research Laboratory in TUBITAK BILGEM [28] as shown in rightmost photograph on Fig. 5. In this design, it is targeted to obtain at least -5 dBi gain and at most 3 dB AR in 65° elevation beamwidth within widest bandwidth as possible. The radiation patterns are measured over azimuth plane, and elevation planes for different ϕ-cuts at some sample frequencies, which are 11.8, 12, 12.3, 13.8, 14, and 14.3 GHz.

In Fig. 7, the simulated and measured azimuth gain patterns at $\theta = 90°$ plane are demonstrated for 11.8 and 14.3 GHz at which maximum gain variations over the azimuth plane is observed within TM and TC bands, respectively. This is expected from the results in Fig. 3 such that the while lowest suppression of TE_{11} mode is observed at 11.8 GHz within the TM band, lowest suppression of TE_{11} and TE_{21} modes is at 14.3 GHz for the TC band. The simulation and measurement patterns over azimuth planes are close to each other in Fig. 7 such that while about 2 dB ripple in the gain is observed in simulation for both bands, they are 2 and 3 dB in measurement for TM and TC bands, respectively. The difference at 14.3 GHz is possibly due to suppression values in the antenna prototype being slightly lower than simulation results given in Fig. 3.

For AR performance in the elevation plane, sample patterns at 12 and 14 GHz are also demonstrated in Fig. 7 for $\phi = 45°$ plane. The simulation and measurement results are consistent that maximum 2 dB AR and 1.5 dB AR within 65° elevation beamwidth are observed in simulation and measurement for 12 and 14 GHz, respectively. AR patterns in the azimuth plane (not given due to limitation in page) show similar results in simulation and measurement. While maximum AR values obtained from both simulation and measurement are almost 2 dB for the TM band, they are 1.5 and 2.5 dB for the TC band.

In Fig. 8, measured elevation gain patterns at ϕ-cuts of 0°, 45°, 90°, and 135° are also given for center frequencies of 12 and 14 GHz. Due to leakage in TM slots, 14 GHz gives higher

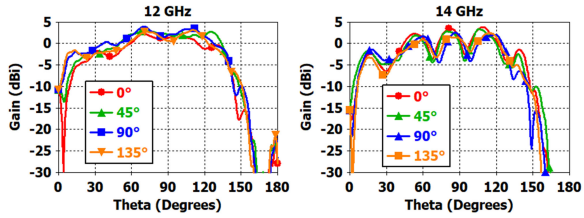

Fig. 8. Measured elevation gain patterns at different ϕ-cuts ($\phi = 0°, 45°, 90°$, and 135° planes) for 12 GHz (left) and 14 GHz (right).

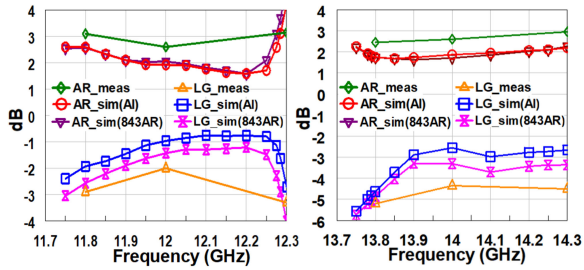

Fig. 9. Measured and simulated lowest gain (LG) and highest AR values of the antenna within 65° elevation beamwidth at TM (left) and TC (right) bands.

TABLE I
COMPARISON OF THE PROPOSED ANTENNA AND OTHER ANTENNAS IN LITERATURE

Study	Frequency (GHz)	10 dB BW	Elevation Beamwidth	LG (dBi)	AR (dB)
[3]	36.85	5.4%	40°	-6	5
[5]	Ka-band	2.0%	65°	-1.5	5.5
[14]	14.5	-	40°	0	3
This Study	11.8-12.3 13.8-14.3	5.0% 8.3%	65° 65°	-3.2 -5	3 3

gain variation and lower minimum gain within 65° elevation beamwidth (57.5° - 122.5°) as compared to 12 GHz.

Finally, LG and highest AR values in elevation beamwidth from 57.5° to 122.5° for TM and TC bands are given in Fig. 9. In a 500 MHz bandwidth for both bands (11.8–12.3 GHz, 13.8–14.3 GHz), minimum -5 dBi gain and 3 dB AR are obtained. The difference for LG values of measurement and simulation (Al) is due to low conductivity of 843AR whose simulation gives better matched results with measurement. The radiation efficiency of the antenna is found to be better than 80% and 70% for simulation with 843AR and measurement. Therefore, conductivity of 843AR might be taken lower than 2.5×10^5 S/m. The loss of MG 843AR has negligible effect on AR results. Thus, differences in AR results are mainly due to production errors (dimensions, not perfectly identical slots). In Table I, a comparison with other single-band antennas gives that the proposed dual-band antenna has the best performance.

IV. CONCLUSION

A dual-band circularly polarized, omnidirectional antenna is proposed. It has one waveguide feed and no dielectric; thus, it is useful for the high-power transceiver (TMTC) on satellite. The antenna is designed and verified at the Ku-band with 3-D printing.

REFERENCES

[1] R. Dybdal, *Communication Satellite Antennas: System Architecture, Technology, and Evaluation*, 1st ed. New York, NY, USA: McGraw-Hill, 2009, pp. 73–82.

[2] L. J. Ippolito, *Satellite Communications System Engineering: Atmospheric Effects, Satellite Link Design and System Performance*, 1st ed. New York, NY, USA: Wiley, 2008, pp. 37–50.

[3] J. L. Masa-Campos, J. M. Fernández, M. Sierra-Pérez, and J. Fernández-Jambrina, "Omnidirectional circularly polarized slot antenna fed by a cylindrical waveguide in millimeter band," *Microw., Opt. Technol. Lett.*, vol. 49, no. 3, pp. 638–642, Mar. 2007.

[4] F. Mayol, M. Padilla, and J. M. Montero, "Turnstile-junction-based omnidirectional antennas for space applications [Antenna Applications]," *IEEE Antennas Propag. Mag.*, vol. 53, no. 3, pp. 255–262, Jun. 2011.

[5] C. B. Top and D. Doğan, "A circularly polarized omni-directional low loss Ka-band slot antenna," in *Proc. IEEE Int. Symp. Antennas Propag.*, Chicago, IL, USA, 2012, pp. 1–2.

[6] K. Sakaguchi and N. Hasebe, "A circularly polarized omnidirectional antenna," in *Proc. 8th Int. Conf. Antennas Propag.,* Edinburgh, U.K., 1993, vol. 1, pp. 477–480.

[7] B. Zhou, J. Geng, X. Bai, L. Duan, X. Liang, and R. Jin, "An omnidirectional circularly polarized slot array antenna with high gain in a wide bandwidth," *IEEE Antennas Wireless Propag. Lett.*, vol. 14, pp. 666–669, 2015.

[8] A. Harmouch *et al.*, "Miniaturized high-gain omnidirectional cylindrical slotted waveguide antenna," *J. Commun. Technol. Electron.*, vol. 60, no. 8, pp. 840–846, Aug. 2015.

[9] C. Turkmen and M. Secmen, "Omnidirectional and circularly polarized slotted antenna array with increased bandwidth performance by using nonidentical waveguide slots," *Radio Sci.*, vol. 53, no. 11, pp. 1406–1418, Nov. 2018.

[10] D. Sivareddy, A. V. G. Subramanyam, U. Prabakaran, V. V. Srinivasan, and V. K. Lakshmeesha, "Ku-band omni antenna system for satellite TTC," in *Proc. IEEE Appl. Electromagn. Conf.*, Kolkata, India, 2011, pp. 1–4.

[11] E.-A. Lee, "A low cross-polarization circularly polarized spacecraft TC&R antenna," in *Proc. IEEE Antennas Propag. Soc. Int. Symp. URSI Nat. Radio Sci. Meeting*, Seattle, WA, USA, 1994, pp. 914–917.

[12] J. Y. Lim *et al.*, "High performance dual-circularly polarized reflector antenna feed," *ETRI J.*, vol. 36, no. 6, pp. 889–893, 2014.

[13] C. Turkmen and M. Secmen, "Circularly polarized hemispherical antennas for telemetry and telecommand applications in satellite communication," in *Proc. 10th Eur. Conf. Antennas Propag.*, Davos, Switzerland, 2016, pp. 1–5.

[14] L. Shafai, S. K. Sharma, and S. Rao, Eds. *Handbook of Reflector Antennas and Feed Systems Volume II: Feed Systems*, Boston, MA, USA: Artech House, 2013, pp. 333–344.

[15] B. Park and J. Lee, "Dual-band omnidirectional circularly polarized antenna using zeroth- and first-order modes," *IEEE Antennas Wireless Propag. Lett.*, vol. 11, pp. 407–410, 2012.

[16] B. Li, S. Liao, and Q. Xue, "Omnidirectional circularly polarized antenna combining monopole and loop radiators," *IEEE Antennas Wireless Propag. Lett.*, vol. 12, pp. 607–610, 2013.

[17] X. Quan, R. Li, and M. M. Tentzeris, "A broadband omnidirectional circularly polarized antenna," *IEEE Trans. Antennas Propag.*, vol. 61, no. 5, pp. 2363–2370, May 2013.

[18] D. Yu, S. Gong, Y. Wan, and W. Chen, "Omnidirectional dual-band dual circularly polarized microstrip antenna using TM01 and TM02 modes," *IEEE Antennas Wireless Propag. Lett.*, vol. 13, pp. 1104–1107, 2014.

[19] W. Cao, A. Liu, B. Zhang, T. Yu, and Z. Qian, "Dual-band spiral patch-slot antenna with omnidirectional CP and unidirectional CP properties," *IEEE Trans. Antennas Propag.*, vol. 61, no. 4, pp. 2286–2289, Apr. 2013.

[20] K. Iigusa, T. Teshirogi, M. Fujita, S.-I. Yamamoto, and T. Ikegami, "A slot-array antenna on a coaxial cylinder with a circularly polarized conical beam," *Electron. Commun. Jpn.*, Part I, vol. 83, no. 3, pp. 74–87, 2000.

[21] M. Khalily, M. R. Kamarudin, M. Mokayef, and M. H. Jamaluddin, "Omnidirectional circularly polarized dielectric resonator antenna for 5.2-GHz WLAN applications," *IEEE Antennas Wireless Propag. Lett.*, vol. 13, pp. 443–446, 2014.

[22] W. W. Li and K. W. Leung, "Omnidirectional circularly polarized dielectric resonator antenna with top-loaded alford loop for pattern diversity design," *IEEE Trans. Antennas Propag.*, vol. 61, no. 8, pp. 4246–4256, Aug. 2013.

[23] Y. M. Pan and K. W. Leung, "Wideband omnidirectional circularly polarized dielectric resonator antenna with parasitic strips," *IEEE Trans. Antennas Propag.*, vol. 60, no. 6, pp. 2992–2997, Jun. 2012.

[24] G. Maral, M. Bousquet, and Z. Sun, *Satellite Communication Systems: Systems, Techniques and Technology*, 6th ed. New York, NY, USA: Wiley, 2020, pp. 543–569.

[25] J. C. S. Chieh, B. Dick, S. Loui, and J. D. Rockway, "Development of a Ku-band corrugated conical horn using 3-D print technology," *IEEE Antennas Wireless Propag. Lett.*, vol. 13, pp. 201–204, 2014.

[26] M. E. Carkaci and M. Secmen, "Design and prototype manufacturing of a feed system for Ku-band satellite communication by using 3D FDM/PLA printing and conductive paint technology," *Int. J. RF Microw. Comput. Aided Eng.*, vol. 30, no. 4, pp. 1–15, Apr. 2020.

[27] *MG Chemicals 843AR Super Shield Silver Coated Copper Conductive Spray Paint*, MG Chemicals, Burlington, ON, Canada. Accessed: Mar. 31, 2021. [Online]. Available: https://www.mgchemicals.com/downloads/tds/tds-843ar-a.pdf

[28] G. Hindman and W.-B. Y. Hanjian, "The implementation of a spherical near-field measurement system in mainland China," in *Proc. Antenna Meas. Techn. Assoc. Conf.*, 1997, pp. 1–5.